Overriding Plate Thickness as a Controlling Factor for Trench Retreat Rates in Narrow Subduction Zones

Pedro J. Gea[1,2] , Flor de Lis Mancilla[1,2] , Ana M. Negredo[3,4] , and Jeroen van Hunen[5]

[1]Department of Theoretical Physics and Cosmology, University of Granada, Granada, Spain, [2]Andalusian Institute of Geophysics, University of Granada, Granada, Spain, [3]Department of Earth Physics and Astrophysics, Complutense University of Madrid, Madrid, Spain, [4]Institute of Geosciences IGEO (CSIC, UCM), Madrid, Spain, [5]Department of Earth Sciences, Durham University, Durham, UK

Abstract Slab width is a significant factor in controlling subduction zone dynamics, particularly the retreat velocities, which tend to decrease with wider slabs. However, observations of natural narrow subduction zones reveal no correlation between slab width and trench velocities. This suggests that other factors may exert a greater influence. In this study, we employ 3D numerical subduction models to systematically assess the impact of slab width, strength of slab coupling to the lateral plate (LP), and overriding plate (OP) thickness on trench kinematics and geometry. Our models focus on narrow slabs (400–1,200 km), and the results demonstrate that, in the case of narrow subduction zones, the slab width has little effect on trench migration rates and the viscous coupling at the lateral slab edge is only important for very narrow subduction zones (≤800 km). Conversely, the OP thickness emerges as a crucial factor, with increasing plate thickness leading to a strong decrease in trench velocities. These findings provide an explanation for the observed trench velocities in natural narrow subduction zones, where an inverse relationship with OP thickness is evident. Furthermore, our study reveals that not only slab width, but also the OP thickness and the slab coupling to the LP, significantly influence trench geometry. Strong lateral coupling promotes the formation of concave trench geometries, while thick overriding plates favor the development of "w"-shaped geometries. Overall, a comprehensive understanding of subduction processes necessitates considering the interplay between slab width, OP thickness, and slab coupling to the LP.

Plain Language Summary Subduction zones are the main drivers of plate tectonics and control much of the seismic and volcanic activity on Earth. For that reason, subduction processes have been widely studied in the last few decades. Because of the limited amount of available data, one of the key techniques has been numerical modeling. Some earlier models have shown that the velocity of the trench (long region marking where subduction starts) is affected by the width of the subduction zone, but this is not observed for narrow subduction zones in nature. In this work, we model 3D narrow subduction systems and find that the thickness of the unsubducted overriding plate (OP) affects trench velocities much more than the width of the subduction zone: the thicker the plate, the slower the trench motion. Moreover, the thickness of the OP affects the shape that the trench develops during progressive subduction. Our models explain some key observations in Earth's narrow subduction zones and help to better understand subduction processes.

1. Introduction

Subducting slabs are considered to be the main drivers of plate motion and flow in Earth's mantle (Davies & Richards, 1992; Forsyth & Uyeda, 1975) and the wide variety of slab morphologies observed in the Earth's interior (e.g., Bijwaard et al., 1998; Chang et al., 2015; Fukao et al., 2001; Goes et al., 2017; Li et al., 2019; van der Hilst et al., 1991, 1995; van der Meer et al., 2018; Widiyantoro et al., 1999; Zhao, 2001) reveals the dependence of subduction processes on many parameters. Thus, much effort has been put in the last few decades into understanding the main factors controlling slab dynamics (e.g., Billen, 2008; Funiciello et al., 2003, 2004; Gerya, 2022; Guillaume et al., 2021; Jadamec & Billen, 2012; Piromallo et al., 2006; Schellart, 2004; Stegman et al., 2010; van Hunen & Allen, 2011). Previous geodynamic modeling studies have shown the influence of several physical parameters on subduction dynamics, such as the slab thickness (e.g., Bellahsen et al., 2005; Capitanio & Morra, 2012; F. Chen et al., 2022; Funiciello et al., 2008; Irvine & Schellart, 2012; Stegman et al., 2010), the subducting plate (SP) length (e.g., Holt & Becker, 2016; Xue et al., 2020), the mantle rheology (e.g., Holt & Becker, 2016; Pusok et al., 2018), the strength of the overriding plate (OP) (e.g., Butterworth et al., 2012; Hertgen

Writing – review & editing: Flor de Lis Mancilla, Ana M. Negredo, Jeroen van Hunen

et al., 2020; Holt et al., 2015; Meyer & Schellart, 2013; Rodríguez-González et al., 2014; Sharples et al., 2014), the slab-mantle viscosity contrast (e.g., Funiciello et al., 2008; Schellart, 2008; Stegman et al., 2010), the coupling at the subduction-interface (e.g., Behr et al., 2022; Duarte et al., 2013; Čížková & Bina, 2013, 2019) or the mechanical boundary conditions (e.g., Z. Chen et al., 2015; Funiciello et al., 2004). All these studies highlight the complexity of subduction, which makes this process still incompletely understood in their key aspects (e.g., Gerya, 2022).

Among the factors controlling subduction dynamics, the slab width (W) has been shown to be of major importance (Bellahsen et al., 2005; F. Chen et al., 2022; Di Giuseppe et al., 2008; Guillaume et al., 2010, 2021; Royden & Husson, 2006; Schellart et al., 2007; Stegman et al., 2006, 2010; Strak & Schellart, 2016). Earlier geodynamic studies have distinguished three types of trench curvature depending on slab width: concave toward the OP side for narrow slabs ($W \leq 1,500$ km), "w"-shaped (also referred to as sublinear) for intermediate width slabs ($W \sim 2,000$–$3,000$ km) and convex toward the OP for wide slabs ($W \geq 4,000$ km) (Schellart et al., 2007; Stegman et al., 2010; Strak & Schellart, 2016), although the exact values differentiating these regimes depend somewhat on the specific conditions. In addition, the slab dip angle seems to be controlled by W, increasing (producing steeper slabs) with wider subducting plates (Schellart, 2004; Strak & Schellart, 2016). W also controls the subduction-induced mantle flow (Piromallo et al., 2006; Stegman et al., 2006), causing faster and more localized mantle upwellings near the lateral slab edges for wider slabs (Strak & Schellart, 2016). Regarding the slab kinematics, previous studies have shown that the trench retreat velocity (V_T) decreases as the slab becomes wider (F. Chen et al., 2022; Schellart, 2004; Schellart et al., 2007; Stegman et al., 2006), with wider subduction zones showing negligible trench retreat in their centers (Schellart et al., 2007). All these studies provide useful insights that help to understand the effect of W on subduction processes. However, most of these model setups that specifically focused on slab width did not incorporate an OP, which is known to affect subduction dynamics significantly (e.g., Butterworth et al., 2012; Capitanio et al., 2010; Z. Chen et al., 2015; Duarte et al., 2013; Hertgen et al., 2020; Magni, 2019; Magni et al., 2014; Rodríguez-González et al., 2014; Yamato et al., 2009). Additionally, as we will discuss in this work, the inverse dependence of V_T on W predicted by some models is not observed in natural narrow subduction zones, suggesting that other factors may play a more relevant role on trench retreat velocities when narrow subduction zones are involved. Incorporating an OP in subduction models can help to better understand the effect of W on V_T and the dominant factors controlling trench retreat rates in narrow subduction zones.

In this study, we have conducted self-consistent 3D numerical models of narrow subduction zones including the subducting and surrounding plates (lateral and overriding) to systematically evaluate the effect of slab width, OP thickness (T_{OP}) and coupling of the slab with the lateral plate (LP) on trench motion. Based on our geodynamic models and a comparison with observations in nature, this work provides new insights on the factors dominating trench retreat velocities in narrow subduction zones.

2. Methods

2.1. Numerical Method

The simulations have been performed with version 2.4.0 of the finite-element code ASPECT (Advanced Solver for Problems in Earth's ConvecTion) (Bangerth et al., 2022; Gassmöller et al., 2018; Heister et al., 2017; Kronbichler et al., 2012). We have used the Boussinesq approximation to solve the coupled conservation equations for mass, momentum and energy, which assumes that the density is constant in all equations except in the buoyancy term of the momentum equation (right hand term in Equation 2):

$$\nabla \cdot \mathbf{u} = 0 \tag{1}$$

$$-\nabla \cdot 2\mu\dot{\varepsilon}\left(\mathbf{u}\right) + \nabla P = \rho\mathbf{g} \tag{2}$$

$$\rho_o c_p\left(\frac{\partial T}{\partial t} + \mathbf{u} \cdot \nabla T\right) - \nabla \cdot k\nabla T = \rho_o H \tag{3}$$

where $\dot{\varepsilon} = \frac{1}{2}\left(\nabla\mathbf{u} + \nabla\mathbf{u}^T\right)$ is the strain rate tensor, ρ is the density, μ is the viscosity, P is the pressure, $\mathbf{u}$ is the velocity, $\mathbf{g}$ is the gravitational acceleration, c_p is the specific heat, T is the temperature, k is the thermal conductivity, ρ_o is the density at a reference temperature T_o and H is the radiogenic heating, which is neglected in our models.
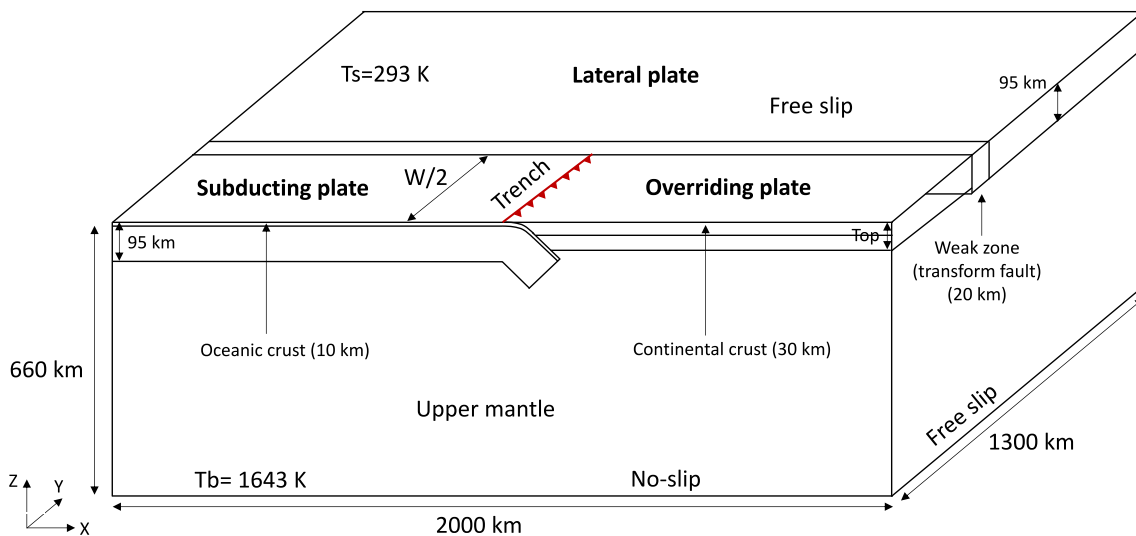
Figure 1. Three-dimensional model setup and boundary conditions. The setup includes a subducting plate (SP), an overriding plate (OP), and a lateral plate (LP). The SP is made of oceanic crust 10 km thick and lithosphere 85 km thick. The OP consists of a 30 km thick crust and 40 km thick lithosphere in the reference model. The LP is comprised of 95 km thick lithosphere and it is separated from the OP and SP by a 20 km wide weak zone (i.e., transform fault). W indicates slab width and the red line with triangles marks the initial trench position at $x = 1,000$ km. The trench is plotted for the whole subduction zone in Figures 3, 4, and 6. The temperature is fixed to 293 K at the top boundary and 1,643 K at the bottom boundary. All boundaries are free-slip except the bottom of the box, where a no-slip condition is applied to simulate the upper-lower mantle discontinuity. Note that only half of the subduction zone is modeled due to the symmetry of the problem.

Besides these equations, ASPECT solves the advection of compositional fields c_i, which are used to track materials and their properties throughout the simulations:

$$\frac{\partial c_i}{\partial t} + \mathbf{u} \cdot \nabla c_i = 0 \tag{4}$$

2.2. Model Setup

The initial 3-D model setup is shown in Figure 1. The initial geometry has been built using the Geodynamic World Builder version 0.4.0 (Fraters et al., 2019, 2021) and it measures 2,000 × 1,300 × 660 km in the *x*, *y*, and *z* directions. The width of the model box (1,300 km) is such that the separation between the lateral slab edge and the lateral sidewall is always at least half-width of the slab and larger than the depth of the upper mantle (660 km) in order to minimize the influence of the lateral wall on subduction dynamics (Schellart et al., 2007, 2010). We have tested the effect of the distance between the lateral slab edge and the sidewall by running our model with the widest slab (*W*/2 = 600 km) with a box width of 2,600 km and have found that the trench retreat velocities just show a maximum increase of 0.2 cm/yr (~6%) throughout the model evolution, thus confirming that our results are not significantly affected by the sidewall boundary condition. We use an adaptive mesh refinement (AMR) that allows us to locally increase the mesh resolution in areas of strong gradients of viscosity, temperature and/or composition, resulting in a maximum resolution of 7.8 × 5 × 2.6 km and a minimum resolution of 62.5 × 20.3 × 20.6 km. The highest mesh resolution is achieved within the SP and OP to accurately resolve the subduction zone interface, while the broadest meshing is only reached in the deep part of the upper mantle. Because the *XZ* plane at *y* = 0 is a plane of symmetry (Figure 1), we only model one half of the subduction zone, as usually done in subduction model setups (e.g., F. Chen et al., 2022; Király et al., 2017; Piromallo et al., 2006; Schellart & Moresi, 2013; Sharples et al., 2014; Stegman et al., 2010; Yamato et al., 2009).

The initial geometry consists of an incipient subduction system with a 220 km-long slab and a dip angle of 40°. In this way, no external forces are imposed and the subduction is self-driven by the negative buoyancy of the slab. The subducting plate (SP) has an initial length of 1,000 km and is comprised of weak crust 10 km thick and lithospheric mantle 85 km thick. The weak crust has a low viscosity of 10^{20} Pa s to allow for the decoupling of the slab from the OP and to facilitate subduction. This crust mimics a weak layer of sedimentary material at the top of the SP. The OP is also 1,000 km long and has an initial thickness of 70 km in the reference model, consisting of a 30 km thick continental crust and a 40 km thick lithospheric mantle. To avoid unnecessary model complexity, the

Table 1
Model Parameters

Symbol	Parameter name	Value	Units
Upper mantle rheology			
A	Exponential prefactor	$5.97 \cdot 10^{-16}$	$\text{Pa}^{-1} \ \text{m}^3 \ \text{s}^{-1}$
E	Activation energy	335	$\text{kJ} \ \text{mol}^{-1}$
V	Activation volume	$4 \cdot 10^{-6}$	$\text{m}^3 \ \text{mol}^{-1}$
d	Grain size	10^{-2}	m
m	Grain size exponent	3	–
Overriding plate crust rheology			
A	Exponential prefactor	$5 \cdot 10^{-11}$	$\text{Pa}^{-1} \ \text{m}^3 \ \text{s}^{-1}$
E	Activation energy	170	$\text{kJ} \ \text{mol}^{-1}$
V	Activation volume	0	–
d	Grain size	10^{-2}	m
m	Grain size exponent	3	–
Other model parameters			
ρ_{um}	Upper mantle density	3,300	$\text{kg} \ \text{m}^{-3}$
ρ_{cc}	Overriding continental crust density	2,900	$\text{kg} \ \text{m}^{-3}$
ρ_{oc}	Oceanic crust density	3,300	$\text{kg} \ \text{m}^{-3}$
ρ_{TF}	Transform fault density	3,300	$\text{kg} \ \text{m}^{-3}$
μ_{oc}	Oceanic crust viscosity	10^{20}	Pa s
μ_{min}	Minimum viscosity	10^{19}	Pa s
μ_{max}	Maximum viscosity	$1.57 \cdot 10^{23}$	Pa s
c_p	Specific heat	1,250	$\text{J} \ \text{kg}^{-1} \ \text{K}^{-1}$
κ	Thermal diffusivity	$0.8 \cdot 10^{-6}$	$\text{m}^2 \ \text{s}^{-1}$
α	Thermal expansion coefficient	$3.5 \cdot 10^{-5}$	K^{-1}
R	Gas constant	8.31	$\text{J} \ \text{K}^{-1} \ \text{mol}^{-1}$
g	Gravitational acceleration	9.8	$\text{m} \ \text{s}^{-2}$
T_0	Reference temperature	293	K

LP is completely made of lithosphere 95 km thick, without any compositional stratification. We prescribe a weak zone (i.e., transform fault) 20 km wide of 10^{20} Pa s in the reference model as a mechanical coupling of the LP with the other plates. The trench is initially located at $x = 1,000$ km, and we use particles placed along its length to track its movement over time.

The SP and OP are fixed at their trailing edges, simulating a subduction zone that is attached to much larger and relatively immobile plates. This scenario is different from plates with free trailing edges, corresponding with minimum resistance to lateral motion at spreading ridges. Most narrow subduction systems (as we will further discuss) are part of much larger and relatively stationary subducting and OPs. Therefore, the SP-OP-fixed scenario is well representative of most narrow subduction zones (e.g., Z. Chen et al., 2015; Yamato et al., 2009). Additionally, we have carried out some selected experiments with a free OP to examine its effect on subduction dynamics (see the Supporting Information S1).

The initial temperature profile increases linearly from 293 K at the surface to 1,643 K at the lithosphere-asthenosphere boundary. For the top and bottom boundaries we use Dirichlet temperature conditions. Mechanical boundary conditions are free-slip for all boundaries, except for the bottom of the box where a no-slip condition is imposed to model the upper-lower mantle discontinuity. This discontinuity is characterized by a factor of 10–100 viscosity increase (Davies & Richards, 1992; Kaufmann & Lambeck, 2000), which is simulated in our models as an impenetrable barrier to flow. This assumption is motivated by computational constraints and by the fact that narrow slabs that subduct through trench retreat, such as those modeled in this work, tend to stagnate at the 660 km discontinuity (e.g., Funiciello et al., 2003; Goes et al., 2017; Schellart et al., 2007).

2.3. Rheology

We use a diffusion creep rheology in which the viscosity is given by:

$$\mu = \frac{1}{2A} d^m \exp\left(\frac{E + PV}{RT}\right) \tag{5}$$

where A is a prefactor of the equation, d is the grain size, m is the grain size exponent, E is the activation energy, V is the activation volume and R is the gas constant.

For the upper mantle (asthenosphere and lithospheric mantle) we use rheological parameters from wet olivine (Hirth & Kohlstedt, 2003). With these parameters, we obtain a viscosity of $1.57 \cdot 10^{20}$ Pa s at a depth of 150 km. For the OP crust we adopt rheological parameters from wet anorthite feldspar (Bürgmann & Dresen, 2008). The viscosity is capped by a preset minimum and a maximum viscosity of 10^{19} and $1.57 \cdot 10^{23}$ Pa s (1,000 times the upper mantle viscosity at a depth of 150 km), respectively, to preserve numerical stability. For the oceanic crust, we adopt a low constant viscosity of 10^{20} Pa s. A low viscosity of 10^{20} Pa s is also used in the transform fault of the reference model as a weak mechanical coupling at the lateral slab edge. All model parameters are listed in Table 1.

3. Results

3.1. Effect of Slab Width and Coupling With the Lateral Plate

In order to focus on narrow subduction zones, we systematically changed the slab width with respect to the reference model (Experiment 2 in Table S1 in the Supporting Information S1) in the range of 400–1,200 km (experiments 1–5 in Table S1 in Supporting Information S1). For each experiment, we varied the mechanical coupling at the lateral slab edge by changing the viscosity of the transform fault (μ_{TF}). In addition to the value
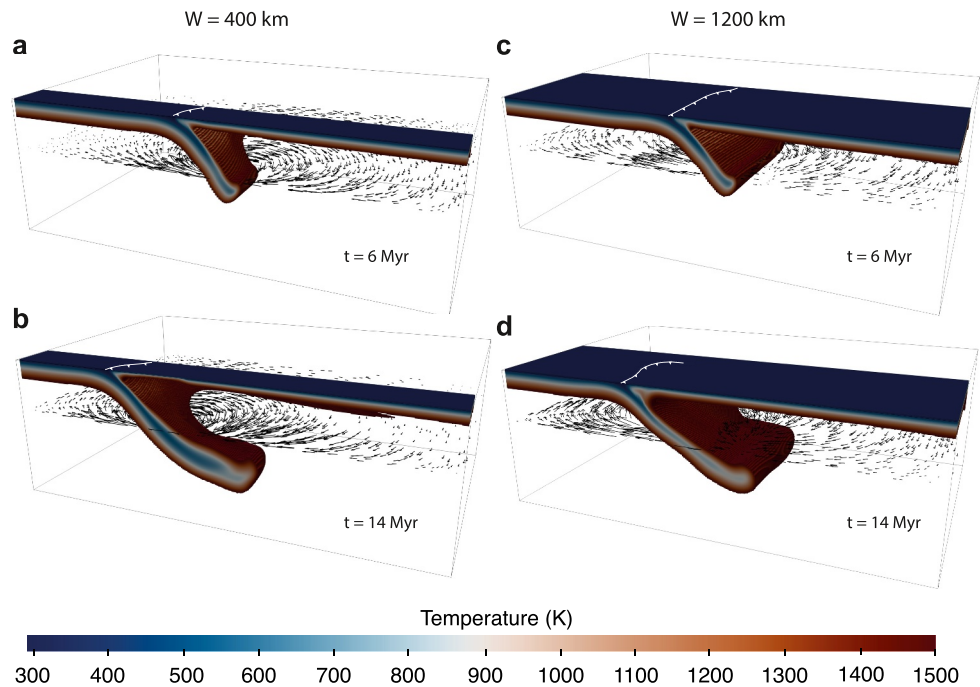
Figure 2. 3D perspective view of the subduction zone for (a, b) $W = 400$ km and (c, d) $W = 1,200$ km. The figures are cutouts of the temperature between 293 and 1,500 K. White lines with triangles on the surface mark the trench position. Black arrows show the horizontal velocity field around the slab at 250 km depth. Note that the lateral plate (LP) is shown as transparent. The trench in panel (d) seems not to be connected to the LP due to some amount of subducting plate shortening in the trench-parallel direction, which is not captured in the temperature cutouts.

$\mu_{TF} = 10^{20}$ Pa s used in the reference model, we tried $\mu_{TF} = 10^{21}$ Pa s (experiments 6–10 in Table S1 in Supporting Information S1) and $\mu_{TF} = 10^{22}$ Pa s (experiments 11–15 in Table S1 in Supporting Information S1).

The subduction dynamics is similar in all the experiments. Initially, the slab freely sinks into the upper mantle due to the density contrast between the SP and the sub-lithospheric mantle and the slab dip angle increases (Figures 2a and 2c). During the sinking phase, the trench retreat velocities quickly increase (Figure 3d), accompanied by slab rollback and inducing toroidal flow around the slab edges (Figure 2). All models show the maximum V_T when the slab tip reaches ∼400 km depth. Thereafter, trench velocities slightly decrease due to the interaction of the slab tip with the deep viscous upper mantle, and approach a roughly constant value (Figure 3d). The high trench retreat rates during subduction lead to the slab lying down horizontally above the deep viscous part of the mantle (Figures 2b and 2d).

Figure 3 shows the influence of SP width on trench shape and kinematics. Models develop two types of trench geometries in the center of the subduction zone depending on W. The trench in models with $W \leq 1,000$ km shows a concave geometry toward the OP, with the trench in the center of the subduction zone retreating faster than its edges (Figures 3a and 3b). This characteristic geometry is attained earlier in models with smaller W. For example, the concave geometry for $W = 400$ km is almost achieved in 2 Myr, while for $W = 600$ km it is not attained until 10 Myr (Figures 3a and 3b). For the model with $W = 1,200$ km, the trench geometry is almost rectilinear in its center with concave edges up to ∼8 Myr, and thereafter adopts a "w"-shape, with retreat velocities being higher in between the lateral slab edge and the center of the subduction zone (Figure 3c).

Trench retreat velocities do not change significantly with the slab widths tested in this work. During the first time steps (0–4 Myr), the trench steadily retreats with similar velocities in all cases. Afterward, trench velocities reach a maximum and finally approach a roughly steady value (Figure 3d). The highest steady velocity is found for $W = 600$ km (∼4.3 cm/yr) and decreases for wider slabs up to a steady velocity of ∼2.9 cm/yr for $W = 1,200$ km (Figure 3d). The highest maximum trench velocity reached during each simulation is found for $W = 400$ km (∼4.9 cm/yr) and slightly decreases for wider slabs (Figure 3d).
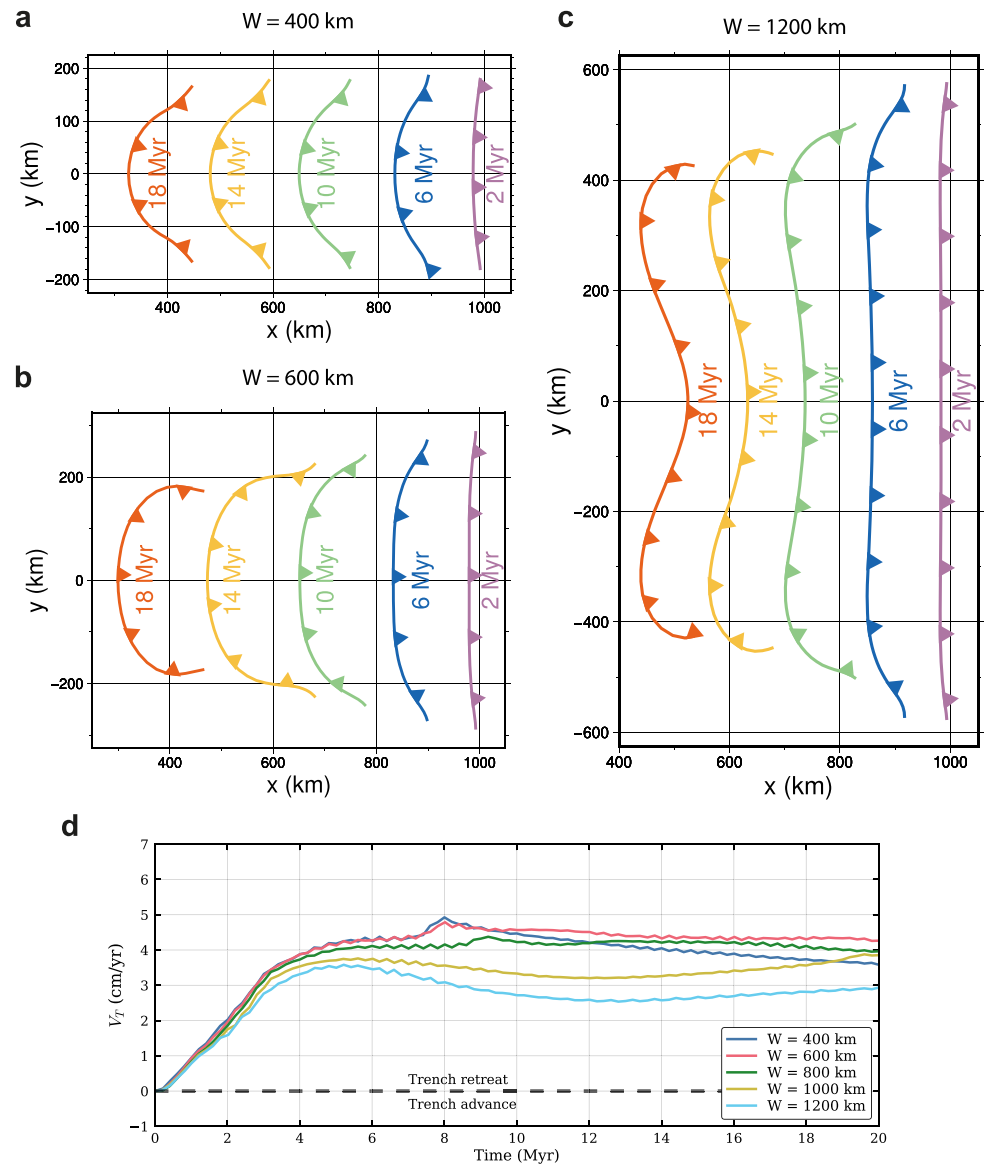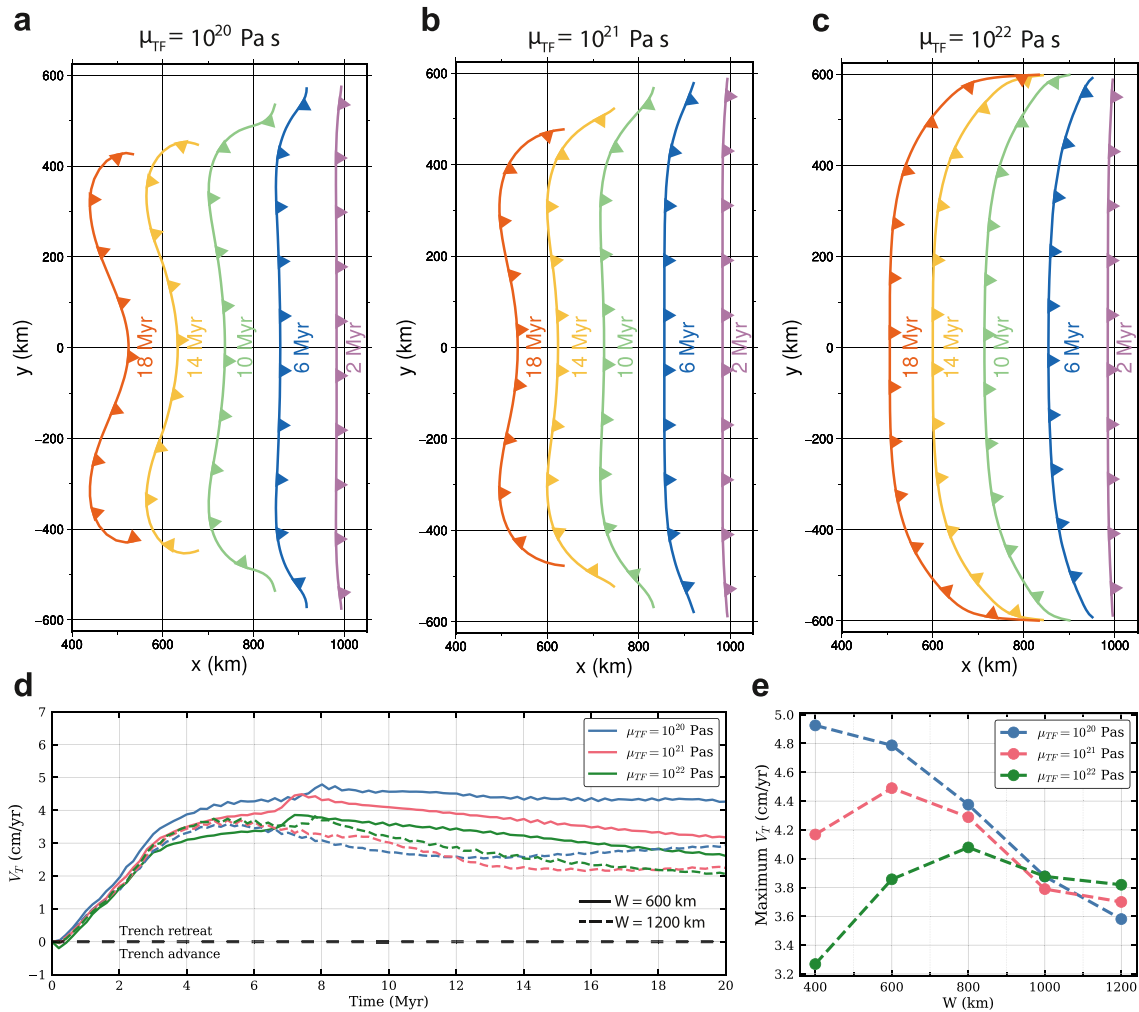
Figure 3. (a–c) Evolution of the subduction trench for three simulations with (a) $W = 400$ km, (b) $W = 600$ km, and (c) $W = 1,200$ km. Note that the entire trench is plotted but we only model half of the subduction zone. (d) V_T over time (measured in the center of the subduction zone) for simulations with different W.

Concerning the mechanical coupling of the slab with the LP, we find that the model with $W = 1,200$ km exhibits different trench geometries depending on the viscosity of the transform fault: we obtain a "w"-shaped trench for a weak coupling ($\mu_{TF} = 10^{20}$ Pa s) (Figure 4a) while a concave trench is developed for a strong coupling ($\mu_{TF} = 10^{22}$ Pa s) (Figure 4c). For the intermediate case ($\mu_{TF} = 10^{21}$ Pa s), we obtain a behavior in between those of the two previous models. The trench remains approximately straight with concave edges and only starts to develop a "w"-shape after ~14 Myr (Figure 4b). A weak lateral coupling leads to some amount of trench shortening in the trench-parallel direction (Figures 3a–3c and 4a), in contrast with models with a strong lateral coupling (Figure 4c; see discussion by Yamato et al. (2009) about trench shortening).

The increase in the viscous resistance at the lateral slab edge causes the trench retreat velocity at the center of the subduction zone to decrease for $W \leq 800$ km, but does not change significantly for $W \geq 800$ km (Figures 4d and 4e). Decreases of ~1.7 and ~1 cm/yr in the maximum trench retreat velocity are observed for $W = 400$ km and $W = 600$ km respectively when the viscosity increases from $\mu_{TF} = 10^{20}$ Pa s to $\mu_{TF} = 10^{22}$ Pa s, while only maximum differences of ~0.2 cm/yr are observed for $W = 1,200$ km (Figure 4e). Additionally, the highest

Figure 4. (a–c) Evolution of the subduction trench for three simulations with $W = 1{,}200$ km and (a) $\mu_{TF} = 10^{20}$ Pa s, (b) $\mu_{TF} = 10^{21}$ Pa s, and (c) $\mu_{TF} = 10^{22}$ Pa s. Note that the entire trench is plotted but we only model half of the subduction zone. (d) V_T over time (measured in the center of the subduction zone) for simulations with different μ_{TF}. Solid lines indicate models with $W = 600$ km and dashed lines indicate models with $W = 1{,}200$ km. (e) Maximum V_T at the center of the subduction zone for different W and different μ_{TF}.

maximum of V_T at the center of the subduction zone is found for $W = 400$ km when the viscosity of the transform fault is $\mu_{TF} = 10^{20}$ Pa s, but for $W = 600$ km when $\mu_{TF} = 10^{21}$ Pa s and for $W = 800$ when $\mu_{TF} = 10^{22}$ Pa s (Figure 4e).

3.2. Effect of Overriding Plate Thickness

We have varied the OP thickness with respect to the reference model in the range of 40–100 km to study its effect on trench motion (Experiments 2 and 16–21 in Table S1 in Supporting Information S1). During the free sinking phase, thin OPs promote fast slab rollback with small dip angles (Figure 5a) while a thick OP leads to the slab sinking almost vertically without rollback (Figure 5c). Consequently, the toroidal mantle flow around the slab is less intense for thicker OPs. The sustained high retreat velocities during all the simulations with a thin OP lead to an elongated flat-lying slab with a very shallow dip angle (Figure 5b). In contrast, for thick OPs, the slab pull force increases as the slab sinks vertically, progressively increasing the retreat velocity and resulting in a stepped slab with its deepest part becoming flattened (Figure 5d).

As for the trench geometry, the trench develops a concave shape for all OP thicknesses (Figures 6a–6d) except for $T_{OP} = 100$ km, where a "w"-shape develops after about 10 Myr of evolution (Figure 6b). Significant trench lateral shortening is also observed as T_{OP} increases (Figure 6b).
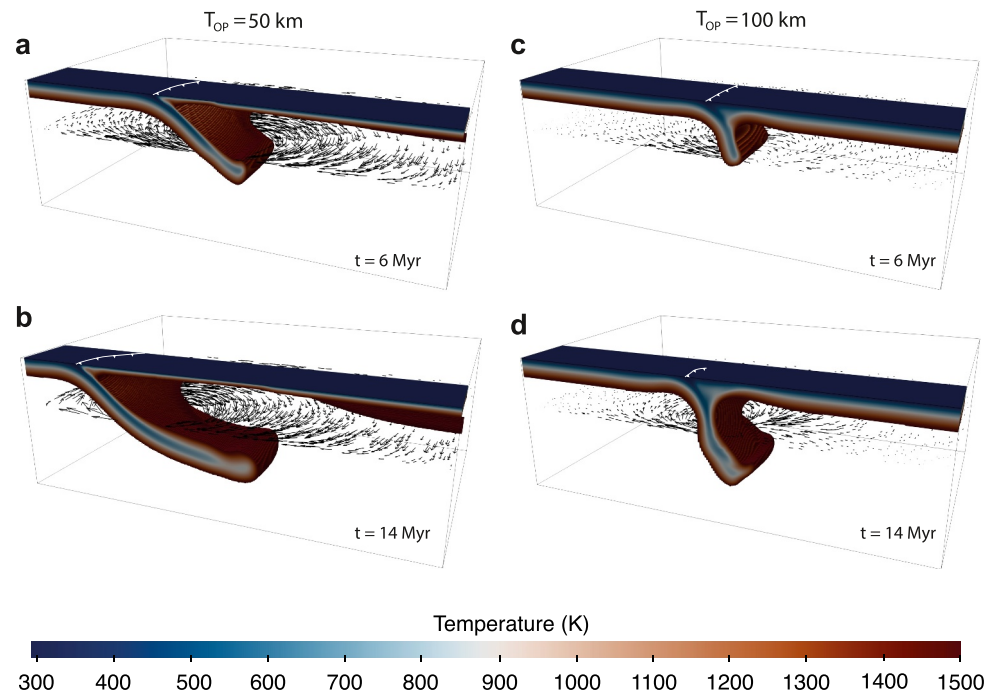
Figure 5. 3D perspective view of the subduction zone for (a, b) $T_{OP} = 50$ km and (c, d) $T_{OP} = 100$ km. The figures are cutouts of the temperature between 293 and 1,500 K. White lines with triangles on the surface mark the trench position. Black arrows show the horizontal velocity field around the slab at 250 km depth. Note that the lateral plate is shown as transparent. See comment about trench representation in the caption of Figure 2.

The trench retreat velocity significantly decreases with thicker OPs (Figure 6e). The maximum V_T decreases from 6.6 cm/yr for $T_{OP} = 40$ km to 4.3 cm/yr for $T_{OP} = 80$ km (Figure 6e). We observe local peaks of trench velocities for the models with $T_{OP} = 40$ km and $T_{OP} = 50$ km at 16–18 Myr and 18–20 Myr respectively, which are likely caused by transient changes in the mantle flow. Short periods of trench advance at the beginning of the simulation occur for $T_{OP} \geq 70$ km. The time during which these models undergo trench advance also increases with the T_{OP}: 2 Myr for $T_{OP} = 100$ km and less than 1 Myr for $T_{OP} = 80$ km (Figure 6e).

4. Discussion

4.1. Comparison With Previous Studies

Our geodynamic models provide new insights into the effect of W, OP thickness and viscous resistance at the lateral slab edge on trench kinematics, and directly complements previous work on this topic. The numerical models of Schellart et al. (2007) and Stegman et al. (2010) suggest values of $W \leq 1,500$ km, $W \sim 2,000$–$3,000$ km and $W \geq 4,000$ km leading to concave, "w"-shaped and convex trenches, respectively, while the analog models of Strak and Schellart (2016) indicate values of $W = 2,000$–$2,500$ km and $W \geq 3,000$ for "w"-shaped and convex geometries respectively. Király et al. (2017) tested plate widths of 1,000, 1,500, and 2,000 km and their models predict concave geometries for the narrow case ($W = 1,000$ km) and "w"-shaped trenches for the wider cases ($W = 1,500$ km and $W = 2,000$ km). In contrast, the analog modeling of Guillaume et al. (2021) predicts concave and "w"-shaped geometries for much wider slabs ($W = 2,000$ and $W = 4,000$ km respectively). Similarly, the recent 3-D spherical shell numerical models of F. Chen et al. (2022) place the transition from concave trenches to "w"-shaped geometries at $W = 2,400$ km for their reference case. Our results do not show convex geometries, which is expected as we focus only on narrow subduction zones and these geometries are found for very wide slabs (Schellart et al., 2007; Strak & Schellart, 2016). We do, however, identify two of the three types of trench geometries identified by Schellart et al. (2007), Stegman et al. (2010), and Strak and Schellart (2016), but our models show a "w"-shaped geometry for a narrower slab ($W = 1,200$ km, Figure 3c) than in previous studies ($W \geq 1,500$ km). These discrepancies may be partly explained by the far-field boundary conditions applied to the SP. In the models of Schellart et al. (2007), Stegman et al. (2010), Strak and Schellart (2016), and F. Chen
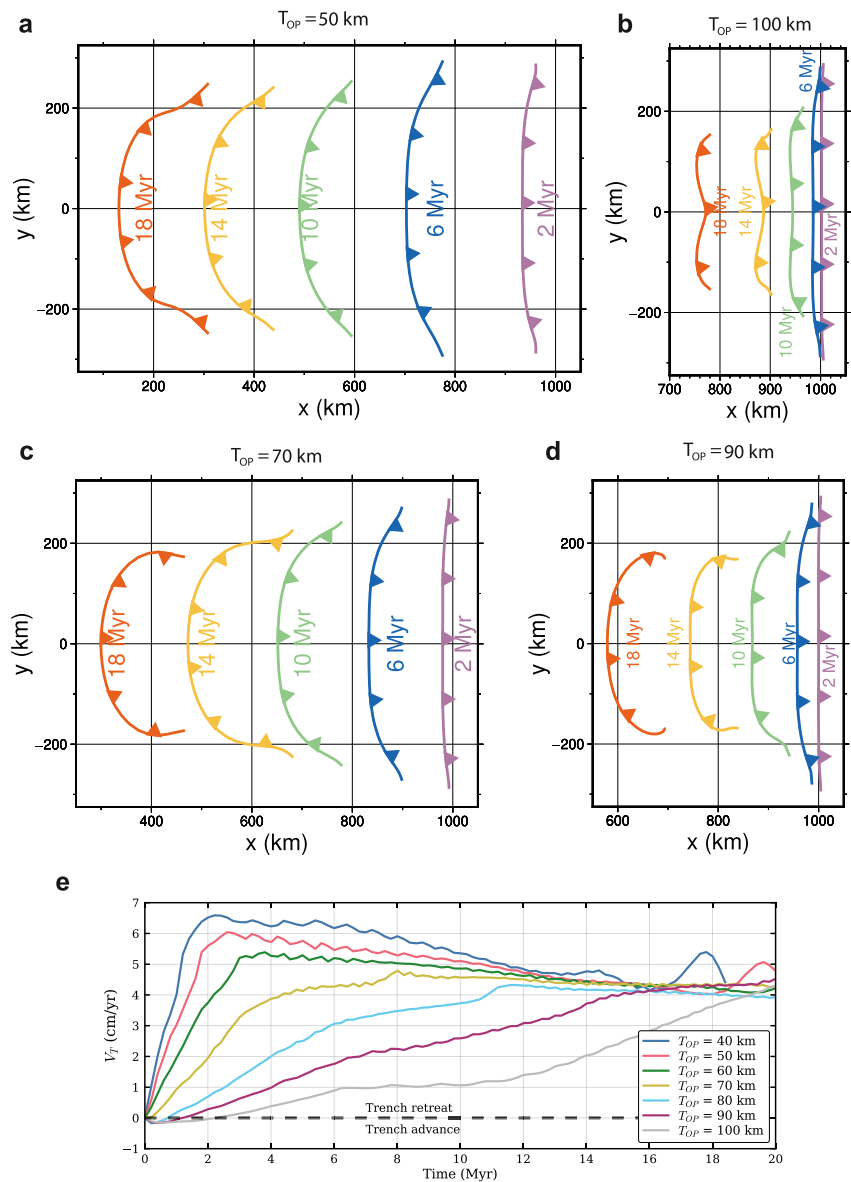
Figure 6. (a–d) Evolution of the subduction trench for four simulations with $W = 600$ km and (a) $T_{OP} = 50$ km, (b) $T_{OP} = 100$ km, (c) $T_{OP} = 70$ km, and (d) $T_{OP} = 90$ km. Note that the entire trench is plotted but we only model half of the subduction zone. (e) V_T over time (measured in the center of the subduction zone) for simulations with different T_{OP}.

et al. (2022), the SP was free to move at its trailing edge (which is more appropriate for wide slabs), while in our models it is fixed (a suitable condition for narrow slabs). In the case of a fixed SP, the subduction process is primarily governed by slab rollback, while a free trailing edge allows the SP to advance toward the trench. The models of Király et al. (2017) and Guillaume et al. (2021) both used fixed subducting plates at their trailing edges, but only the findings of Király et al. (2017) ("w"-shaped trenches for $W = 1,500$ km) are close to the results of this work ("w"-shaped trenches for $W = 1,200$ km). Discrepancies may come from the use of different viscosity ratios between the slab and the upper mantle, but another likely factor that could explain these variations is the influence of the OP, which was not included in these previous studies: our results show that increasing T_{OP} in models with the same slab width promote "w"-shaped trenches (Figure 6b).

Regarding trench migration velocities, previous modeling studies have found that V_T decreases with increasing W (e.g., F. Chen et al., 2022; Schellart et al., 2007; Stegman et al., 2006). However, this behavior is not maintained for narrow subduction zones. Our results show a direct dependence of V_T on W for $W \leq 600$ km when the

mechanical coupling of the slab with the LP is moderate ($\mu_{TF} = 10^{21}$ Pa s) and for $W \leq 800$ km when the coupling is stronger ($\mu_{TF} = 10^{22}$ Pa s) (Figure 4e). This positive correlation between V_T and W has also been suggested in previous works for $W \leq 500$–600 km (Schellart, 2004; Stegman et al., 2006) and for $W \leq \sim 1{,}000$ km (Strak & Schellart, 2016). Our models using an intermediate coupling ($\mu_{TF} = 10^{21}$ Pa s) are in agreement with the results of Stegman et al. (2006) finding a maximum retreat velocity for $W = 600$ km. The discrepancy on the W showing maximum V_T between the present work and previous studies suggests a dependence on different model parameters and setup. For example, our models show that the W for which V_T peaks increases as the viscous resistance at the lateral slab edge becomes stronger (Figure 4e). More research is needed to clarify the dynamics and factors affecting this phenomenon. Here we propose that a peak V_T is observed in Figure 4e due to an energy balance (Magni et al., 2014) between the available gravitational potential energy of the slab E_{pot} and the energy required for frictional dissipation in the mantle $E_{diss,m}$ and at the transform fault $E_{diss,TF}$. For relatively wide slabs ($W \geq 800$ km), $E_{diss,TF}$ is relatively unimportant, E_{pot} linearly increases with slab width, while $E_{diss,m}$ increases faster than E_{pot}. Therefore, trench retreat is slower for wider slabs as the frictional dissipation in the mantle becomes dominant. For narrow slabs ($W \leq 800$ km), E_{pot} and $E_{diss,m}$ are both small, and $E_{diss,TF}$ becomes dominant. Since E_{pot} decreases for narrowing slabs, while $E_{diss,TF}$ is independent of slab width, narrow slabs retreat slower than wider slabs for the range of $W \leq 800$ km.

The effect of the strength of transform faults on trench kinematics remains poorly studied and the coupling of the slab with the LP is usually assumed to be either weak (e.g., Chertova et al., 2018; Király et al., 2021) or strong (e.g., Yamato et al., 2009). Govers and Wortel (2005) made the first study investigating the dynamics at the subduction zone edges based on observations in nature and numerical models. Later on, Hale et al. (2010) evaluated with 3D numerical subduction models how the strength at the lateral slab edge affects the subduction dynamics. Their models showed that increasing the viscous resistance at the transform fault results in lower trench retreat velocities and more prominent trench curvatures, which was also found by Nijholt and Govers (2015). The recent modeling of Schliffke et al. (2022) further highlights the importance of the transform fault strength in subduction dynamics, showing that back-arc ridge jumps depend on the ratio of transform fault versus OP strengths. The results of Hale et al. (2010) are in agreement with our work showing that a strong coupling with the LP increases viscous resistance at the lateral slab edge, enhancing concave trench geometries (Figures 4a–4c) and reduces the trench retreat velocity for $W \leq 800$ km. However, the fact that the three curves in Figure 4e tend to converge with W approaching 1,200 km suggests that effect of the strength of lateral coupling on V_T is only significant for very narrow subduction zones.

Finally, the significant decrease of V_T with increasing T_{OP} reported in Figure 6e demonstrates the strong impact of the OP thickness on trench retreat velocities. This result is in agreement with previous 3D and 2D models (Butterworth et al., 2012; Gea et al., 2023; Hertgen et al., 2020; Sharples et al., 2014; Yamato et al., 2009) finding that thin/weak OP favors faster trench velocities and rollback compared to a thick/strong OP. This result is enhanced by the fixed boundary condition of the OP at its trailing edge. With a fixed-OP condition, slab rollback is entirely accommodated by OP extension, and thus stronger (thicker) OPs will provide more resistance to extension and, hence, to trench retreat. This is very different from a scenario with a free OP, where slab rollback will be accommodated by both OP extension and OP motion toward the trench. For example, the SP-OP-free models of Meyer and Schellart (2013) found fast trench retreat velocities for both thin and thick OP models and showed that increasing the thickness of the OP just retards trench retreat, which is gradually further accommodated by trenchward OP motion. Other models, though, have found that increasing the thickness of the OP reduces rollback rates, regardless of the condition of the OP at its trailing edge, but with a fixed OP enhancing the dependence of trench retreat velocities on the mechanical properties of the OP (Capitanio et al., 2010; Holt et al., 2015). Our supplementary models with a free OP support these results, showing smaller but still significant decreases in retreat velocities with increasing T_{OP} (see Figure S4 in Supporting Information S1).

The short periods of trench advance found in this work for $T_{OP} \geq 70$ km (Figure 6e) are also consistent with the models of Sharples et al. (2014) showing that trench advance only occurs in models with thick and/or strong OPs. The impact of the OP thickness on slab dip angle has also been studied in previous models, some finding that the slab dip angle does not change significantly (e.g., Meyer & Schellart, 2013), while others reporting an increase in slab dip angle at depth with increasing T_{OP} (e.g., Holt et al., 2015; Sharples et al., 2014). Our model results show that T_{OP} does have an effect on slab dip angle through its control on trench retreat velocities: thin OP enhance high trench retreat velocities resulting in small slab dip angles (Figure 5a), while a reduction of retreat velocities due to thicker OP results in an increase of slab dip angle (Figure 5c). The analog models of Meyer and Schellart (2013)
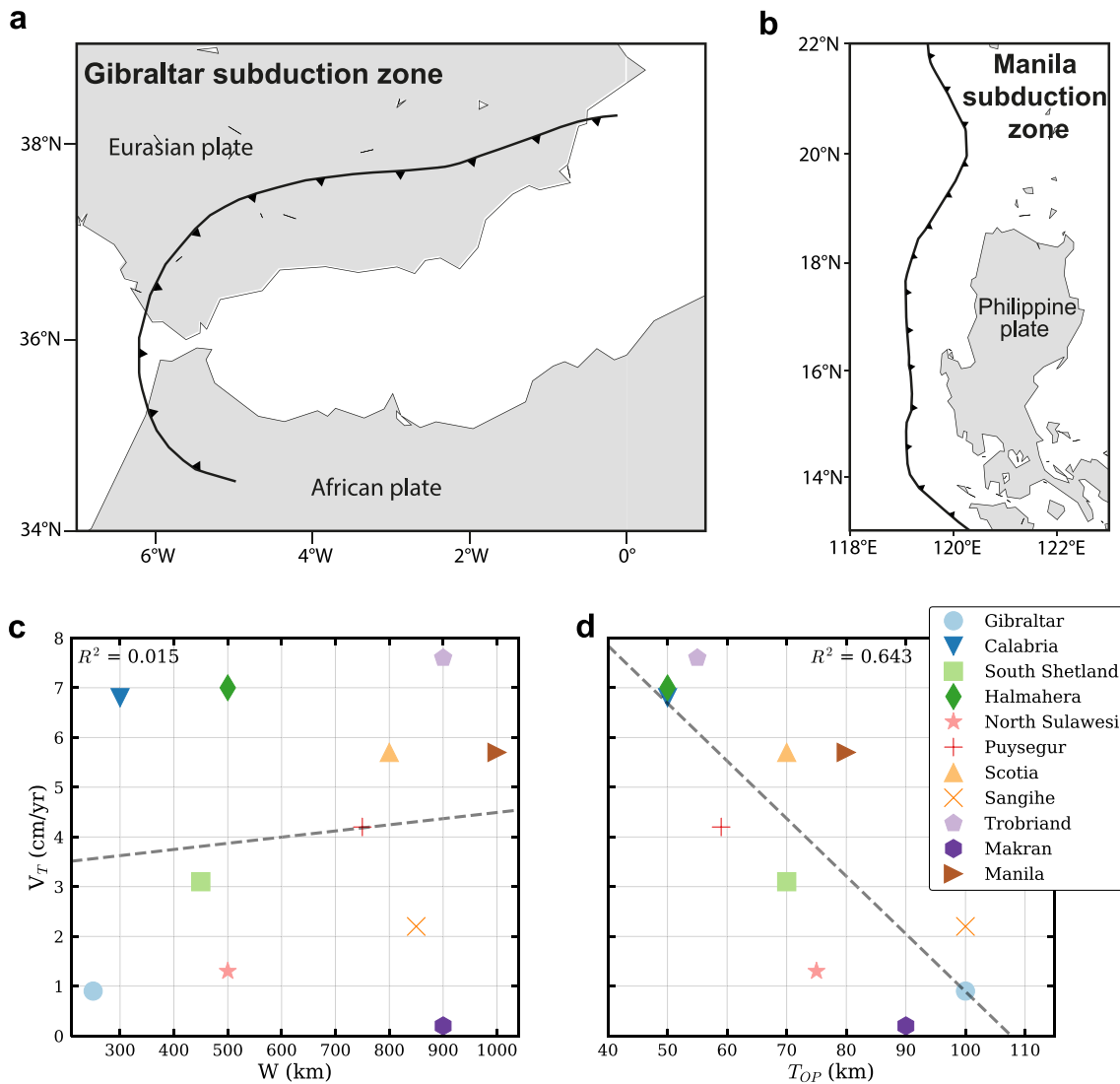
Figure 7. (a, b) Subduction fronts at present-day for the (a) Gibraltar subduction system (from Gutscher et al. (2012)) and the (b) Manila subduction zone (from Qiu et al. (2019)). (c) V_T against W for all subduction zones in Earth with $W \leq 1,000$ km (data from Schellart et al. (2007)). (d) V_T against T_{OP} for all subduction zones in Earth with $W \leq 1,000$ km (data can be found in Table S2 in Supporting Information S1). Note: the T_{OP} plotted values are subjected to significant uncertainty, which in turn depends on the estimation method. The reader is referred to the main text for a more detailed discussion on this point. Gray dashed lines are the least-squares linear best-fit lines and R^2 is the coefficient of determination.

also showed that the trench curvature decreases as T_{OP} increases. Although this is not observed in our models (Figure 6), we do find that the thickness of the OP affects the trench geometry, with an OP 100 km thick resulting in a "w"-shaped trench.

4.2. Comparison With Nature

Natural subduction zones on Earth are influenced by a large number of factors that are not included in our models, such as slabs of non-uniform age, complex slab morphologies or plate velocities. Similarly, interaction of subduction zones on Earth with mantle flow coming from nearby subduction zones elsewhere or from other processes such as mantle plumes can also affect subduction evolution. Thus, comparing our results with observations on Earth should be approached with caution, being aware of the inherent limitations. Nevertheless, our geodynamic model predictions are useful to explain some observations on natural narrow subduction zones.

The concave trench geometries predicted by our geodynamic models are widely observed on Earth for narrow subduction zones such as Scotia, South Shetland, Calabria or Gibraltar (Figure 7a). Our results have

demonstrated that including an OP promotes the formation of "w"-shaped geometries. For example, the model with $W = 1,200$ km and $\mu_{TF} = 10^{20}$ Pa s develops a "w"-shaped trench (Figure 3c) for much smaller W than any of the previous studies not incorporating an OP (e.g., F. Chen et al., 2022; Schellart et al., 2007; Stegman et al., 2010; Strak & Schellart, 2016). Increasing the thickness of the OP has also been shown to affect the geometry of the trench, with an OP 100 km thick leading to a "w"-shaped geometry (Figure 6b). This effect of the OP could explain why some natural subduction zones of narrow to intermediate widths develop "w"-shapes. For example, the Manila trench ($W = 1,000$ km) has a geometry between concave and "w"-shaped (Figure 7b). The main difference with our results is that the Manila trench is convex toward the OP at its northernmost part, while for our models the trench geometry is symmetric and convex in its center. We attribute these differences to the use of an idealized model setup with uniform subducting and OPs, which results in symmetric trenches. Additionally, the Manila subduction zone is affected by the Ryukyu subduction system and the convex geometry in its northernmost extremity may be explained by slab-slab interactions with the Ryukyu slab (Király et al., 2016).

The decrease in V_T with increasing W observed in the present work for $W \geq 800$ km (Figures 3d and 3e) and in previous works (e.g., F. Chen et al., 2022; Royden & Husson, 2006; Schellart et al., 2007; Stegman et al., 2006) is in general agreement with observations in narrow and wide subduction zones. This result explains why narrow subduction zones (e.g., Calabria, South Shetland, Halmahera) exhibit relatively high V_T, while wide subduction zones (e.g., Melanesia, South America) are essentially stationary (Schellart et al., 2007). However, when this comparison is restricted to narrow subduction zones, no correlation between W and V_T is observed ($R^2 = 0.015$, Figure 7c). For the same slab width ($\sim$900 km), the Makran subduction zone has a V_T of 0.2 cm/yr while the Trobriand system has a V_T of 7.6 cm/yr (Schellart et al., 2007). Our results showing that W has little effect on V_T for narrow subduction zones, with variations in V_T less than $\sim$2 cm/yr (Figure 3d), are in agreement with the lack of correlation between W and V_T observed in nature and provide an explanation for these observations.

Conversely, our models reveal that the effect of OP thickness is much stronger, showing an inverse dependence of V_T on T_{OP} (Figure 6e). This negative correlation is also observed in nature for narrow subduction zones ($R^2 = 0.643$, Figure 7d) and brings an explanation of why two subduction zones with the same W (e.g., Makran and Trobriand) show such different V_T. Nevertheless, it is essential to acknowledge the substantial uncertainty associated with estimating OP thickness in natural settings. The accuracy of OP thickness determination in each subduction zone is inherently related to the specific geophysical method used for its assessment. Receiver functions emerge as the best method for lithosphere thickness estimation, but only two data points, namely Gibraltar (Molina-Aguilera et al., 2019) and South Shetland (Parera-Portell et al., 2021), have been based on receiver function analysis. For the rest of the subduction zones, the data have been based on other, much less accurate geophysical methods, including tectonic reconstruction studies for Calabria (Rosenbaum & Lister, 2004), numerical models that best fit the observations for Halmahera (Zhang et al., 2017) and North Sulawesi (Dong et al., 2022), seismic crustal studies for Puysegur (Shuck et al., 2021) and Makran (Motaghi et al., 2020), mantle tomography studies for Sangihe (Fan & Zhao, 2018), heat flow studies for Trobriand (Martinez et al., 2001) and the global thermochemical model of the lithosphere and underlying upper mantle WINTERC-G for Scotia and Manila (Fullea et al., 2021). Thus, although the negative correlation between V_T and T_{OP} appears evident for narrow subduction zones at first order, the significant uncertainty in the data must be considered. Future studies are needed to better estimate the OP thickness and to further confirm this V_T-T_{OP} correlation.

We note that our far-field boundary conditions (SP-fixed and OP-fixed) limit our results to these specific conditions, which represent a scenario where subduction zones are attached to larger and relatively immobile plates. However, our SP-OP-fixed condition is primarily consistent with the natural examples presented in this study, since most narrow slabs are embedded within larger subducting plates and have a relatively stationary OP. The Mediterranean subduction zones (Gibraltar, Calabria, and Hellenic) are good examples of this scenario, as both Eurasia and Africa are moving much slower than the subduction zones inside. The Makran subduction zone is also comparable to our SP-OP-fixed condition as the slab is embedded within the much larger SP (Arabia) and OP (Eurasia). Among the subduction systems presented in this work, those with an OP moving trenchward at high rates (which ideally would be best comparable to a SP-fixed OP-free scenario) include the subduction zones of Puysegur beneath the overriding Pacific plate, Trobriand beneath the Australian plate, Manila below the Philippine plate and Scotia under the South Sandwich plate. Even in these cases, it is not straightforward that an SP-fixed OP-free condition would be the most applicable to these scenarios because the high velocities of the OPs

may be partly attributed to other nearby subduction zones (e.g., Tonga for Puysegur or the Melanesia subduction zone for Trobriand). In any case, our supplementary models reveal that even including a free OP, the effect of T_{OP} on trench retreat velocities remains more relevant than W for narrow subduction zones (see Figure S4 in Supporting Information S1).

Finally, it is worth noting that although the model setup used in this study includes a continental OP, the qualitative results are also valid for an oceanic OP, as it is the case for some of the above-mentioned natural examples. The thermal thickness and strength of the oceanic lithosphere are directly related to its age, and therefore a thick (old, cold, and strong) oceanic lithosphere will provide more resistance to internal deformation and trench motion than a thin oceanic OP.

4.3. Model Limitations

Our numerical models contain some limitations that should be taken into account. We employ a simplified rheological structure. The advantage of including the three plates and allowing for their relative motions and interaction has the drawback of requiring an increased mesh resolution in the weak zones between the plates. While this is satisfactorily assessed thanks to the AMR feature of ASPECT code, simulations are still expensive in terms of computation time. In order to keep acceptable computation times which allow for a deeper exploration in the parameters space, we used a linear temperature- and pressure- dependent viscosity. The use of simplified rheologies has been shown to satisfactorily reproduce realistic subduction dynamics and slab morphologies (Capitanio et al., 2007; Di Giuseppe et al., 2008; Ribe, 2010; Strak & Schellart, 2018). More complicated (computationally much more expensive) rheologies such as non-linear viscoplastic rheology promote strain localization and back-arc spreading in the OP, resulting in higher rates of trench retreat (Pusok et al., 2018). Still, a thicker and therefore stronger OP would delay or even hinder strain localization compared to a thinner plate and therefore our qualitative results of slower trench retreats for thicker OPs would not change.

We do not consider the effect of nearby subduction zones on our individual subduction models, although the interaction between nearby subduction zones naturally exists in nature. Indeed, it has been shown that slab-slab interactions may influence the trench kinematics, the induced mantle flow, and the deformation of the subduction zones involved (Király et al., 2021). Interactions between narrow slabs in nature include the coupled evolution of the Ryukyu and Manila subduction zones, the divergent double subduction of Halmahera and Sangihe and the recent simultaneous subduction of the Mediterranean slabs. However, we argue that the influence of external mantle flow coming from nearby subduction zones is of secondary importance compared to the negative buoyancy of the slab (Forsyth & Uyeda, 1975).

We fix the trailing edge of the SP and OP (apart from a few free OP models in Supporting Information S1), thereby neglecting LP velocities. In such scenario, the SP subducts almost entirely by slab rollback and is accommodated by extension of the upper plate. This is a simplification of subduction zones in nature, where the plate velocities are not negligible. For example, previous subduction models (and data from subduction zones in nature) have shown that the SP velocity increases with increasing slab width (Schellart et al., 2010). The OP also contributes to the subduction rate, with a global average trench-normal velocity of 0.81 cm/yr (Schellart, 2023). However, most narrow subduction zones, which are the focus of this work, are embedded within much larger and relatively immobile plates, with the subducting and OPs usually having low trench-normal velocities. Therefore, the behavior of narrow subduction zones can be best approximated by the SP-OP-fixed condition that we use in this work (Z. Chen et al., 2015; Yamato et al., 2009).

Our models are restricted to subduction in the upper mantle since the 660-km discontinuity is simulated as an impenetrable barrier, even though it is known that some slabs are able to penetrate into the lower mantle with high dip angles (e.g., Hellenic, Peru) (e.g., Bijwaard et al., 1998; Fukao et al., 2001; van der Hilst et al., 1991). This simplification implies that the interaction of the slab with the upper-lower mantle discontinuity is amplified, for example, by further decelerating the slab sinking. However, previous 3D subduction modeling studies that include a high-viscosity lower mantle have shown that those slabs that subduct primarily by trench retreat tend to stagnate and flatten above the discontinuity (e.g., Funiciello et al., 2003; Griffiths et al., 1995; Schellart et al., 2007; Sharples et al., 2014; Stegman et al., 2006, 2010). Therefore, the no-slip boundary condition at the bottom of the models to simulate the 660-km discontinuity seems to be a reasonable approximation for our models in which the subducting slabs are dominated by trench retreat.

5. Conclusions

The self-consistent 3-D numerical subduction models presented in this work shed light on some factors (slab width, OP thickness and viscous coupling at the lateral slab edge) controlling trench kinematics in narrow subduction zones, and help to explain some observations of natural subduction processes. As opposed to what happens in wide subduction zones, our models show that the slab width has little effect on trench retreat velocities for narrow subduction zones, which explains the lack of correlation between these parameters observed in nature. In contrast, from our models and observations in nature we conclude that the thickness of the OP is the main controlling factor on trench retreat velocities for narrow subduction zones, with velocities strongly decreasing as the thickness increases. Stronger coupling to the LP has been found to increase the trench curvature, favoring concave geometries, but its effect on decreasing trench retreat velocities is only significant for very narrow subduction zones. Finally, our work reveals that the inclusion of an OP plays an important role in modulating trench geometries, facilitating the formation of "w"-shaped geometries, which are predicted for smaller slab widths than in previous studies.

Data Availability Statement

The version 2.4.0 of ASPECT used in this study is available at (Bangerth et al., 2022). All the information and parameters of the models of this work can be found in the Methods section. The files required to reproduce our simulations are available at (Gea, 2023).

References

Bangerth, W., Dannberg, J., Fraters, M., Gassmoeller, R., Glerum, A., Heister, T., et al. (2022). Aspect v2.4.0 [Software]. Zenodo. https://doi.org/10.5281/zenodo.6903424

Behr, W. M., Holt, A., Becker, T. W., & Faccenna, C. (2022). The effects of plate interface rheology on subduction kinematics and dynamics. *Geophysical Journal International*, *230*(2), 796–812. https://doi.org/10.1093/gji/ggac075

Bellahsen, N., Faccenna, C., & Funiciello, F. (2005). Dynamics of subduction and plate motion in laboratory experiments: Insights into the "plate tectonics" behavior of the earth. *Journal of Geophysical Research*, *110*(B1), B01401. https://doi.org/10.1029/2004JB002999

Bijwaard, H., Spakman, W., & Engdahl, E. R. (1998). Closing the gap between regional and global travel time tomography. *Journal of Geophysical Research*, *103*(B12), 30055–30078. https://doi.org/10.1029/98JB02467

Billen, M. I. (2008). Modeling the dynamics of subducting slabs. *Annual Review of Earth and Planetary Sciences*, *36*(1), 325–356. https://doi.org/10.1146/annurev.earth.36.031207.124129

Bürgmann, R., & Dresen, G. (2008). Rheology of the lower crust and upper mantle: Evidence from rock mechanics, geodesy, and field observations. *Annual Review of Earth and Planetary Sciences*, *36*(1), 531–567. https://doi.org/10.1146/annurev.earth.36.031207.124326

Butterworth, N., Quevedo, L., Morra, G., & Müller, D. (2012). Influence of overriding plate geometry and rheology on subduction. *Geochemistry, Geophysics, Geosystems*, *13*(6), Q06W15. https://doi.org/10.1029/2011GC003968

Capitanio, F., & Morra, G. (2012). The bending mechanics in a dynamic subduction system: Constraints from numerical modelling and global compilation analysis. *Tectonophysics*, *522–523*, 224–234. https://doi.org/10.1016/j.tecto.2011.12.003

Capitanio, F., Morra, G., & Goes, S. (2007). Dynamic models of downgoing plate-buoyancy driven subduction: Subduction motions and energy dissipation. *Earth and Planetary Science Letters*, *262*(1), 284–297. https://doi.org/10.1016/j.epsl.2007.07.039

Capitanio, F., Stegman, D., Moresi, L., & Sharples, W. (2010). Upper plate controls on deep subduction, trench migrations and deformations at convergent margins. *Tectonophysics*, *483*(1–2), 80–92. https://doi.org/10.1016/j.tecto.2009.08.020

Chang, S.-J., Ferreira, A. M. G., Ritsema, J., van Heijst, H. J., & Woodhouse, J. H. (2015). Joint inversion for global isotropic and radially anisotropic mantle structure including crustal thickness perturbations. *Journal of Geophysical Research: Solid Earth*, *120*(6), 4278–4300. https://doi.org/10.1002/2014JB011824

Chen, F., Davies, D. R., Goes, S., Suchoy, L., & Kramer, S. C. (2022). How slab age and width combine to dictate the dynamics and evolution of subduction systems: A 3-D spherical study. *Geochemistry, Geophysics, Geosystems*, *23*(11), e2022GC010597. https://doi.org/10.1029/2022GC010597

Chen, Z., Schellart, W. P., & Duarte, J. (2015). Overriding plate deformation and variability of fore-arc deformation during subduction: Insight from geodynamic models and application to the Calabria subduction zone. *Geochemistry, Geophysics, Geosystems*, *16*(10), 3697–3715. https://doi.org/10.1002/2015GC005958

Chertova, M. V., Spakman, W., & Steinberger, B. (2018). Mantle flow influence on subduction evolution. *Earth and Planetary Science Letters*, *489*, 258–266. https://doi.org/10.1016/j.epsl.2018.02.038

Čížková, H., & Bina, C. R. (2013). Effects of mantle and subduction-interface rheologies on slab stagnation and trench rollback. *Earth and Planetary Science Letters*, *379*, 95–103. https://doi.org/10.1016/j.epsl.2013.08.011

Čížková, H., & Bina, C. R. (2019). Linked influences on slab stagnation: Interplay between lower mantle viscosity structure, phase transitions, and plate coupling. *Earth and Planetary Science Letters*, *509*, 88–99. https://doi.org/10.1016/j.epsl.2018.12.027

Davies, G. F., & Richards, M. A. (1992). Mantle convection. *The Journal of Geology*, *100*(2), 151–206. https://doi.org/10.1086/629582

Di Giuseppe, E., van Hunen, J., Funiciello, F., Faccenna, C., & Giardini, D. (2008). Slab stiffness control of trench motion: Insights from numerical models. *Geochemistry, Geophysics, Geosystems*, *9*(2), Q02014. https://doi.org/10.1029/2007GC001776

Dong, M., Lü, C., Zhang, J., & Hao, T. (2022). Downgoing plate-buoyancy driven retreat of North Sulawesi trench: Transition of a passive margin into a subduction zone. *Geophysical Research Letters*, *49*(23), e2022GL101130. https://doi.org/10.1029/2022GL101130

Duarte, J. C., Schellart, W. P., & Cruden, A. R. (2013). Three-dimensional dynamic laboratory models of subduction with an overriding plate and variable interplate rheology. *Geophysical Journal International*, *195*(1), 47–66. https://doi.org/10.1093/gji/ggt257

Fan, J., & Zhao, D. (2018). Evolution of the southern segment of the Philippine trench: Constraints from seismic tomography. *Geochemistry, Geophysics, Geosystems*, *19*(11), 4612–4627. https://doi.org/10.1029/2018GC007685

Forsyth, D., & Uyeda, S. (1975). On the relative importance of the driving forces of plate motion. *Geophysical Journal International*, *43*(1), 163–200. https://doi.org/10.1111/j.1365-246X.1975.tb00631.x

Fraters, M., Thieulot, C., van den Berg, A., & Spakman, W. (2019). The geodynamic World builder: A solution for complex initial conditions in numerical modeling. *Solid Earth*, *10*(5), 1785–1807. https://doi.org/10.5194/se-10-1785-2019

Fraters, M., Thieulot, C., van den Berg, A., & Spakman, W. (2021). The geodynamic World builder v0.4.0. *Zenodo*. https://doi.org/10.5281/zenodo.5014808

Fukao, Y., Widiyantoro, S., & Obayashi, M. (2001). Stagnant slabs in the upper and lower mantle transition region. *Reviews of Geophysics*, *39*(3), 291–323. https://doi.org/10.1029/1999RG000068

Fullea, J., Lebedev, S., Martinec, Z., & Celli, N. L. (2021). WINTERC-G: Mapping the upper mantle thermochemical heterogeneity from coupled geophysical–petrological inversion of seismic waveforms, heat flow, surface elevation and gravity satellite data. *Geophysical Journal International*, *226*(1), 146–191. https://doi.org/10.1093/gji/ggab094

Funiciello, F., Faccenna, C., & Giardini, D. (2004). Role of lateral mantle flow in the evolution of subduction systems: Insights from laboratory experiments. *Geophysical Journal International*, *157*(3), 1393–1406. https://doi.org/10.1111/j.1365-246X.2004.02313.x

Funiciello, F., Faccenna, C., Giardini, D., & Regenauer-Lieb, K. (2003). Dynamics of retreating slabs: 2. Insights from three-dimensional laboratory experiments. *Journal of Geophysical Research*, *108*(B4), 2207. https://doi.org/10.1029/2001JB000896

Funiciello, F., Faccenna, C., Heuret, A., Lallemand, S., Di Giuseppe, E., & Becker, T. (2008). Trench migration, net rotation and slab–mantle coupling. *Earth and Planetary Science Letters*, *271*(1), 233–240. https://doi.org/10.1016/j.epsl.2008.04.006

Gassmöller, R., Lokavarapu, H., Heien, E., Puckett, E. G., & Bangerth, W. (2018). Flexible and scalable particle-in-cell methods with adaptive mesh refinement for geodynamic computations. *Geochemistry, Geophysics, Geosystems*, *19*(9), 3596–3604. https://doi.org/10.1029/2018GC007508

Gea, P. J. (2023). Pedrogea08/gea_et_al2023gcubed: New release [Dataset]. Zenodo. https://doi.org/10.5281/zenodo.10057966

Gea, P. J., Negredo, A. M., & Mancilla, F. D. L. (2023). The Gibraltar slab dynamics and its influence on past and present-day Alboran domain deformation: Insights from thermo-mechanical numerical modelling. *Frontiers in Earth Science*, *11*, 995041. https://doi.org/10.3389/feart.2023.995041

Gerya, T. (2022). Numerical modeling of subduction: State of the art and future directions. *Geosphere*, *18*(2), 503–561. https://doi.org/10.1130/GES02416.1

Goes, S., Agrusta, R., van Hunen, J., & Garel, F. (2017). Subduction-transition zone interaction: A review. *Geosphere*, *13*(3), 644–664. https://doi.org/10.1130/GES01476.1

Govers, R., & Wortel, M. (2005). Lithosphere tearing at step faults: Response to edges of subduction zones. *Earth and Planetary Science Letters*, *236*(1), 505–523. https://doi.org/10.1016/j.epsl.2005.03.022

Griffiths, R. W., Hackney, R. I., & van der Hilst, R. D. (1995). A laboratory investigation of effects of trench migration on the descent of subducted slabs. *Earth and Planetary Science Letters*, *133*(1), 1–17. https://doi.org/10.1016/0012-821X(95)00027-A

Guillaume, B., Funiciello, F., & Faccenna, C. (2021). Interplays between mantle flow and slab pull at subduction zones in 3D. *Journal of Geophysical Research: Solid Earth*, *126*(5), e2020JB021574. https://doi.org/10.1029/2020JB021574

Guillaume, B., Funiciello, F., Faccenna, C., Martinod, J., & Olivetti, V. (2010). Spreading pulses of the Tyrrhenian sea during the narrowing of the Calabrian slab. *Geology*, *38*(9), 819–822. https://doi.org/10.1130/G31038.1

Gutscher, M.-A., Dominguez, S., Westbrook, G., Le Roy, P., Rosas, F., Duarte, J., et al. (2012). The Gibraltar subduction: A decade of new geophysical data. *Tectonophysics*, *574–575*, 72–91. https://doi.org/10.1016/j.tecto.2012.08.038

Hale, A. J., Gottschaldt, K.-D., Rosenbaum, G., Bourgouin, L., Bauchy, M., & Mühlhaus, H. (2010). Dynamics of slab tear faults: Insights from numerical modelling. *Tectonophysics*, *483*(1), 58–70. (Convergent plate margin dynamics: New perspectives from structural geology, geophysics and geodynamic modelling). https://doi.org/10.1016/j.tecto.2009.05.019

Heister, T., Dannberg, J., Gassmöller, R., & Bangerth, W. (2017). High accuracy mantle convection simulation through modern numerical methods. II: Realistic models and problems. *Geophysical Journal International*, *210*(2), 833–851. https://doi.org/10.1093/gji/ggx195

Hertgen, S., Yamato, P., Guillaume, B., Magni, V., Schliffke, N., & van Hunen, J. (2020). Influence of the thickness of the overriding plate on convergence zone dynamics. *Geochemistry, Geophysics, Geosystems*, *21*(2), e2019GC008678. https://doi.org/10.1029/2019GC008678

Hirth, G., & Kohlstedt, D. (2003). Rheology of the upper mantle and the mantle wedge: A view from the experimentalists. In *Washington DC American geophysical union geophysical monograph series* (Vol. 138, pp. 83–105). https://doi.org/10.1029/138GM06

Holt, A., Becker, T., & Buffett, B. (2015). Trench migration and overriding plate stress in dynamic subduction models. *Geophysical Journal International*, *201*(1), 172–192. https://doi.org/10.1093/gji/ggv011

Holt, A., & Becker, T. W. (2016). The effect of a power-law mantle viscosity on trench retreat rate. *Geophysical Journal International*, *208*(1), 491–507. https://doi.org/10.1093/gji/ggw392

Irvine, D. N., & Schellart, W. P. (2012). Effect of plate thickness on bending radius and energy dissipation at the subduction zone hinge. *Journal of Geophysical Research*, *117*(B6), B06405. https://doi.org/10.1029/2011JB009113

Jadamec, M. A., & Billen, M. I. (2012). The role of rheology and slab shape on rapid mantle flow: Three-dimensional numerical models of the Alaska slab edge. *Journal of Geophysical Research*, *117*(B2), B02304. https://doi.org/10.1029/2011JB008563

Kaufmann, G., & Lambeck, K. (2000). Mantle dynamics, postglacial rebound and the radial viscosity profile. *Physics of the Earth and Planetary Interiors*, *121*(3), 301–324. https://doi.org/10.1016/S0031-9201(00)00174-6

Király, A., Capitanio, F. A., Funiciello, F., & Faccenna, C. (2016). Subduction zone interaction: Controls on arcuate belts. *Geology*, *44*(9), 715–718. https://doi.org/10.1130/G37912.1

Király, A., Capitanio, F. A., Funiciello, F., & Faccenna, C. (2017). Subduction induced mantle flow: Length-scales and orientation of the toroidal cell. *Earth and Planetary Science Letters*, *479*, 284–297. https://doi.org/10.1016/j.epsl.2017.09.017

Király, A., Funiciello, F., Capitanio, F. A., & Faccenna, C. (2021). Dynamic interactions between subduction zones. *Global and Planetary Change*, *202*, 103501. https://doi.org/10.1016/j.gloplacha.2021.103501

Kronbichler, M., Heister, T., & Bangerth, W. (2012). High accuracy mantle convection simulation through modern numerical methods. *Geophysical Journal International*, *191*(1), 12–29. https://doi.org/10.1111/j.1365-246X.2012.05609.x

Li, Z.-H., Gerya, T., & Connolly, J. A. (2019). Variability of subducting slab morphologies in the mantle transition zone: Insight from petrological-thermomechanical modeling. *Earth-Science Reviews*, *196*, 102874. https://doi.org/10.1016/j.earscirev.2019.05.018

Magni, V. (2019). The effects of back-arc spreading on arc magmatism. *Earth and Planetary Science Letters*, *519*, 141–151. https://doi.org/10.1016/j.epsl.2019.05.009

Magni, V., Faccenna, C., van Hunen, J., & Funiciello, F. (2014). How collision triggers backarc extension: Insight into Mediterranean style of extension from 3-D numerical models. *Geology*, *42*(6), 511–514. https://doi.org/10.1130/G35446.1

Martinez, F., Goodliffe, A., & Taylor, B. (2001). Metamorphic core complex formation by density inversion and lower-crust extrusion. *Nature*, *411*(6840), 930-4. https://doi.org/10.1038/35082042

Meyer, C., & Schellart, W. P. (2013). Three-dimensional dynamic models of subducting plate-overriding plate-upper mantle interaction. *Journal of Geophysical Research: Solid Earth*, *118*(2), 775–790. https://doi.org/10.1002/jgrb.50078

Molina-Aguilera, A., de Lis Mancilla, F., Morales, J., Stich, D., Yuan, X., & Heit, B. (2019). Connection between the Jurassic oceanic lithosphere of the Gulf of Cádiz and the Alboran slab imaged by Sp receiver functions. *Geology*, *47*(3), 227–230. https://doi.org/10.1130/G45654.1

Motaghi, K., Shabanian, E., & Nozad-Khalil, T. (2020). Deep structure of the western coast of the Makran subduction zone, se Iran. *Tectonophysics*, *776*, 228314. https://doi.org/10.1016/j.tecto.2019.228314

Nijholt, N., & Govers, R. (2015). The role of passive margins on the evolution of subduction-transform edge propagators (steps). *Journal of Geophysical Research: Solid Earth*, *120*(10), 7203–7230. https://doi.org/10.1002/2015JB012202

Parera-Portell, J. A., de Lis Mancilla, F., Morales, J., Almendros, J., & Jiménez-Morales, V. (2021). Structure of the crust and upper mantle beneath the Bransfield strait (Antarctica) using P receiver functions. *Tectonophysics*, *802*, 228744. https://doi.org/10.1016/j.tecto.2021.228744

Piromallo, C., Becker, T. W., Funiciello, F., & Faccenna, C. (2006). Three-dimensional instantaneous mantle flow induced by subduction. *Geophysical Research Letters*, *33*(8), 956. https://doi.org/10.1029/2005GL025390

Pusok, A., Kaus, B., & Popov, A. (2018). The effect of rheological approximations in 3-D numerical simulations of subduction and collision. *Tectonophysics*, *746*, 296–311. https://doi.org/10.1016/j.tecto.2018.04.017

Qiu, Q., Li, L., Hsu, Y.-J., Wang, Y., Chan, C.-H., & Switzer, A. D. (2019). Revised earthquake sources along manila trench for tsunami hazard assessment in the South China Sea. *Natural Hazards and Earth System Sciences*, *19*(7), 1565–1583. https://doi.org/10.5194/nhess-19-1565-2019

Ribe, N. M. (2010). Bending mechanics and mode selection in free subduction: A thin-sheet analysis. *Geophysical Journal International*, *180*(2), 559–576. https://doi.org/10.1111/j.1365-246X.2009.04460.x

Rodríguez-González, J., Billen, M. I., & Negredo, A. M. (2014). Non-steady-state subduction and trench-parallel flow induced by overriding plate structure. *Earth and Planetary Science Letters*, *401*, 227–235. https://doi.org/10.1016/j.epsl.2014.06.013

Rosenbaum, G., & Lister, G. S. (2004). Neogene and Quaternary rollback evolution of the Tyrrhenian Sea, the Apennines, and the Sicilian Maghrebides. *Tectonics*, *23*(1), TC1013. https://doi.org/10.1029/2003TC001518

Royden, L. H., & Husson, L. (2006). Trench motion, slab geometry and viscous stresses in subduction systems. *Geophysical Journal International*, *167*(2), 881–905. https://doi.org/10.1111/j.1365-246X.2006.03079.x

Schellart, W. P. (2004). Kinematics of subduction and subduction-induced flow in the upper mantle. *Journal of Geophysical Research*, *109*(B7), B07401. https://doi.org/10.1029/2004JB002970

Schellart, W. P. (2008). Kinematics and flow patterns in deep mantle and upper mantle subduction models: Influence of the mantle depth and slab to mantle viscosity ratio. *Geochemistry, Geophysics, Geosystems*, *9*(3), Q09006. https://doi.org/10.1029/2007GC001656

Schellart, W. P. (2023). Chapter 14—Subduction zones: A short review. In J. C. Duarte (Ed.), *Dynamics of plate tectonics and mantle convection* (pp. 321–355). Elsevier. https://doi.org/10.1016/B978-0-323-85733-8.00009-3

Schellart, W. P., Freeman, J., Stegman, D., Moresi, L., & May, D. (2007). Evolution and diversity of subduction zones controlled by slab width. *Nature*, *446*(7133), 308–311. https://doi.org/10.1038/nature05615

Schellart, W. P., & Moresi, L. (2013). A new driving mechanism for backarc extension and backarc shortening through slab sinking induced toroidal and poloidal mantle flow: Results from dynamic subduction models with an overriding plate. *Journal of Geophysical Research: Solid Earth*, *118*(6), 3221–3248. https://doi.org/10.1002/jgrb.50173

Schellart, W. P., Stegman, D. R., Farrington, R. J., Freeman, J., & Moresi, L. (2010). Cenozoic tectonics of western North America controlled by evolving width of Farallon slab. *Science*, *329*(5989), 316–319. https://doi.org/10.1126/science.1190366

Schliffke, N., van Hunen, J., Allen, M. B., Magni, V., & Gueydan, F. (2022). Episodic back-arc spreading centre jumps controlled by transform fault to overriding plate strength ratio. *Nature Communications*, *13*(1), 582. https://doi.org/10.1038/s41467-022-28228-5

Sharples, W., Jadamec, M. A., Moresi, L. N., & Capitanio, F. A. (2014). Overriding plate controls on subduction evolution. *Journal of Geophysical Research: Solid Earth*, *119*(8), 6684–6704. https://doi.org/10.1002/2014JB011163

Shuck, B., Van Avendonk, H., Gulick, S. P. S., Gurnis, M., Sutherland, R., Stock, J., et al. (2021). Strike-slip enables subduction initiation beneath a failed rift: New seismic constraints from Puysegur Margin, New Zealand. *Tectonics*, *40*(5), e2020TC006436. https://doi.org/10.1029/2020TC006436

Stegman, D., Farrington, R., Capitanio, F., & Schellart, W. (2010). A regime diagram for subduction styles from 3-D numerical models of free subduction. *Tectonophysics*, *483*(1), 29–45. (Convergent plate margin dynamics: New perspectives from structural geology, geophysics and geodynamic modelling). https://doi.org/10.1016/j.tecto.2009.08.041

Stegman, D., Freeman, J., Schellart, W. P., Moresi, L., & May, D. (2006). Influence of trench width on subduction hinge retreat rates in 3-D models of slab rollback. *Geochemistry, Geophysics, Geosystems*, *7*(3), 3060. https://doi.org/10.1029/2005GC001056

Strak, V., & Schellart, W. P. (2016). Control of slab width on subduction-induced upper mantle flow and associated upwellings: Insights from analog models. *Journal of Geophysical Research: Solid Earth*, *121*(6), 4641–4654. https://doi.org/10.1002/2015JB012545

Strak, V., & Schellart, W. P. (2018). A subduction and mantle plume origin for Samoan volcanism. *Scientific Reports*, *8*(1), 10424. https://doi.org/10.1038/s41598-018-28267-3

van der Hilst, R. (1995). Complex morphology of subducted lithosphere in the mantle beneath the Tonga trench. *Nature*, *374*(6518), 154–157. https://doi.org/10.1038/374154a0

van der Hilst, R., Engdahl, R., Spakman, W., & Nolet, G. (1991). Tomographic imaging of subducted lithosphere below northwest pacific island arcs. *Nature*, *353*(6339), 37–43. https://doi.org/10.1038/353037a0

van der Meer, D. G., van Hinsbergen, D. J., & Spakman, W. (2018). Atlas of the underworld: Slab remnants in the mantle, their sinking history, and a new outlook on lower mantle viscosity. *Tectonophysics*, *723*, 309–448. https://doi.org/10.1016/j.tecto.2017.10.004

van Hunen, J., & Allen, M. B. (2011). Continental collision and slab break-off: A comparison of 3-D numerical models with observations. *Earth and Planetary Science Letters*, *302*(1), 27–37. https://doi.org/10.1016/j.epsl.2010.11.035

Widiyantoro, S., Kennett, B., & van der Hilst, R. (1999). Seismic tomography with p and s data reveals lateral variations in the rigidity of deep slabs. *Earth and Planetary Science Letters*, *173*(1), 91–100. https://doi.org/10.1016/S0012-821X(99)00216-2

Xue, K., Schellart, W. P., & Strak, V. (2020). Effect of plate length on subduction kinematics and slab geometry: Insights from buoyancy-driven analog subduction models. *Journal of Geophysical Research: Solid Earth*, *125*(11), e2020JB020514. https://doi.org/10.1029/2020JB020514

Yamato, P., Husson, L., Braun, J., Loiselet, C., & Thieulot, C. (2009). Influence of surrounding plates on 3D subduction dynamics. *Geophysical Research Letters*, *36*(7), L07303. https://doi.org/10.1029/2008GL036942

Zhang, Q., Guo, F., Zhao, L., & Wu, Y. (2017). Geodynamics of divergent double subduction: 3-D numerical modeling of a Cenozoic example in the Molucca Sea region, Indonesia. *Journal of Geophysical Research: Solid Earth*, *122*(5), 3977–3998. https://doi.org/10.1002/2017JB013991

Zhao, D. (2001). New advances of seismic tomography and its applications to subduction zones and earthquake fault zones: A review. *Island Arc*, *10*(1), 68–84. https://doi.org/10.1046/j.1440-1738.2001.00291.x